Res Chem Intermed (2018) 44:2703–2717
https://doi.org/10.1007/s11164-018-3255-x

Improved catalytic activity and N_2 selectivity of Fe–Mn–O_x catalyst for selective catalytic reduction of NO by NH_3 at low temperature

Futing Xia[1,2,3] · Zhongxian Song[4] · Xin Liu[4] · Xi Liu[3] · Yinhua Yang[3] · Qiulin Zhang[4] · Jinhui Peng[1,2]

Received: 15 October 2017 / Accepted: 8 January 2018 / Published online: 24 January 2018

Abstract FeO_x, MnO_x and Fe–Mn–O_x catalysts were prepared by the co-precipitation method and used for the selective catalytic reduction (SCR) of NO_x by NH_3 at low temperature. Fe–Mn–O_x catalyst showed the best catalytic activity and above 80% NO_x conversion was obtained at 50–150 °C. Nearly 80% N_2 selectivity of Fe–Mn–O_x catalyst was acquired at the whole temperature range. The excellent low-temperature SCR activity and N_2 selectivity were ascribed to the abundant surface acid sites, the formation of Fe–O–Mn species, co-existence of multiple valence states (Mn^{4+}, Mn^{3+} and Mn^{2+}) and the proper redox ability. In addition, the interaction between Fe and Mn species over the Fe–Mn–O_x catalyst was responsible for the improvement of SCR performance and N_2 selectivity.

Graphical Abstract Fe–Mn–O_x catalysts were prepared by the co-precipitation method and used for the selective catalytic reduction (SCR) of NO_x by NH_3 at low temperature. The formation of Fe–O–Mn species contributed to the co-existence of multiple valence states (Mn^{4+}, Mn^{3+}, Mn^{2+}, Fe^{3+} and Fe^{2+}), resulting in an increase

✉ Futing Xia
xiafuting@163.com

✉ Jinhui Peng
jhpeng@kmust.edu.cn

1 Faculty of Metallurgical and Energy Engineering, Kunming University of Science and Technology, Kunming 650500, China

2 State Key Laboratory of Complex Nonferrous Metal Resources Clean Utilization, Kunming 650093, China

3 Key Laboratory of Resource Clean Conversion in Ethnic Regions, Education Department of Yunnan, Yunnan Minzu University, Kunming 650500, China

4 Faculty of Environmental Science and Engineering, Kunming University of Science and Technology, Kunming 650500, China

in catalytic activity and N_2 selectivity. Besides, the abundance of acid sites was responsible for the superior N_2 selectivity.

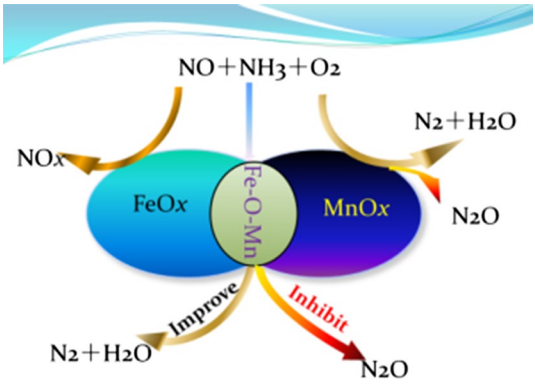

Keywords Fe–Mn–O_x · Selective catalytic reduction · N_2 selectivity · Fe–O–Mn species · Acid sites

Introduction

Nitrogen oxides (NO_x) are the main source of environmental pollution such as the greenhouse effect, acid deposition and photochemical smog, which is harmful to human health and environment [1–3]. The mature de-NO_x technology is selective catalytic reduction of NO by NH_3 (NH_3-SCR), and V_2O_5–WO_3 (or MO_3)/TiO_2 catalysts have been widely used and operated at 300–400 °C in power stations [4, 5]. However, there are still some drawbacks of traditional commercial catalysts, such as the poor low-temperature activity, the formation of N_2O at high temperature and the narrow reaction temperature window (300–400 °C) [6, 7]. Moreover, the NH_3-SCR catalyst bed is placed upstream of dedusting and desulfurization under the reheating the flue gas conditions, resulting in a decrease in the catalytic activity due to the high concentrations of dust and SO_2 [8]. In addition, the temperature of the flue gas after dedusting and desulfurization is in the temperature range of 50–150 °C. Hence, the SCR device is located downstream of the dedusting and desulfurization units, leading to the inferior SCR performance of traditional SCR catalysts at low temperatures (below 150 °C). To solve the above problems, great efforts are made to develop the SCR catalysts with superior low-temperature catalytic performance below 150 °C to avoid gas preheating.

Mn-containing catalysts have been explored and regarded as highly active catalysts for low-temperature NH_3-SCR Co-doping of the other components, phase composition of Mn-containing species, and valence states have been explored for these Mn-containing NH_3-SCR catalysts [9–13]. Cr–MnO_x mixed-oxide catalyst can exhibit excellent SCR activity in the range of 120–220 °C, and the co-existence of

Mn^{4+}–Mn^{3+} plays a crucial role in the improvement of catalytic activity [14]. Thirupathi et al. [15] proved that the high reducibility of MnO_2 phase plays an important role in the superior SCR performance over the nickel-doped Mn/TiO_2 catalyst. Kang et al. [16] reported that Cu–Mn mixed oxides are active at low temperature and the formation of $Cu_{0.01}Mn_{0.25}O_x$ contributes to the improvement of low-temperature catalytic activity. Qi et al. [17, 18] found that MnO_x–CeO_2 catalyst presents above 95% NO_x conversion and excellent resistance to $H_2O + SO_2$ at 150 °C. Above all, the Mn-based catalysts with the excellent low-temperature catalytic activity can be assigned to the superior oxidation ability and various chemical valence states (Mn^{4+}, Mn^{3+} and Mn^{2+}). A proper molar ratio of Mn^{3+}/Mn^{4+} plays a critical role for enhancing NH_3-SCR performance over Mn-based catalysts. Besides, for Mn-based catalysts, the excellent oxidation of NH_3–NO_x (NO and NO_2) can lead to poor N_2 selectivity due to the excellent redox ability, which have restrained its further development in the field of low-temperature catalysis. Therefore, Mn-based catalysts should be improved through modification in order to adjust the N_2 selectivity and low-temperature SCR activity.

Fe_2O_3 is widely employed due to the abundant surface acidity in the NH_3-SCR reaction [19, 20]. It was reported [21] that the surface acidity can be significantly improved by the addition of Fe species and then contributed to the excellent N_2 selectivity. Chen et al. [8] proved that the introduction of Fe species can improve the low-temperature catalytic activity and N_2 selectivity. $FeMnO_x$ mixed-oxide catalysts showed potential catalytic performance at low temperature. Sb et al. [22] also demonstrated that the presence of $Fe_3Mn_3O_8$ phase in $FeMnO_x$ catalyst contributes to the catalytic activity. Low-temperature SCR activity, resistance to $H_2O + SO_2$ and synergetic effect of Fe and Mn have been previously explored [23–25]. However, it deserves further explorations to investigate relationships among the N_2 selectivity, surface acidity and redox properties.

In this work, the FeO_x, Fe–Mn–O_x and MnO_x catalysts are prepared by co-precipitation method and used for selective catalytic reduction of NO with NH_3. The influence of surface acidity and catalyst structure on the catalytic performance of the samples is studied. The catalysts structure, surface acidity, redox ability and SCR activity of the samples are characterized by XRD, Raman, N_2 physisorption, XPS, H_2-TPR and NH_3-TPD.

Experimental

Catalyst synthesis

The FeO_x, Fe–Mn–O_x and MnO_x catalysts were prepared by the co-precipitation method. As for the FeO_x catalyst, the preparation process was as follows: Firstly, $Fe(NO_3)_3{\cdot}9H_2O$ was dissolved in deionized water. Secondly, the ammonia solution (25 wt%) was gradually dripped with continuous stirring for 0.5 h at 25 °C until the pH value reached 10. Afterwards, the precipitates were maintained at 80 °C for 5 h under stirring conditions. Finally, the resulting sample was filtered, washed, and dried at 105 °C overnight, and then it was calcined at 550 °C for 5 h. The obtained solid

powders were denoted as FeO_x. The preparation process of Fe–Mn–O_x (50 wt% FeO_x and 50 wt% MnO_x) and MnO_x catalysts was the same as that of FeO_x catalyst.

Catalytic activity test

The experimental tests were operated in a fixed-bed quartz reactor (8 mm i.d.) with 0.4 mL catalysts. The concentrations of simulated gases were as follows: 5 vol% O_2, 600 ppm NH_3, 600 ppm NO and N_2 as balance gas. The total gas flow rate remained 400 mL/min, corresponding to gas hourly space velocity (GHSV) of 60,000 h^{-1}. The concentration of NO_x (NO and NO_2) was continuously detected by the ECOM·J2KN flue gas analyzer. The N_2O concentration was measured by a gas chromatograph (Fuli, 9790).

Physicochemical characterization

Powder X-ray diffraction (XRD) patterns were carried out on an X-ray diffractometer (Rigaku, D/max-2200, Japan). The scanning range was at 10°–70° at a step of 6° min^{-1}. Raman spectra were carried out on a Renishaw-2000 Raman spectrometer using the 532-nm line of an Ar ion laser as the excitation source. N_2 adsorption–desorption experiments were operated using a Tristar II 3020 automated gas sorption system. The samples were outgassed at 400 °C for 3 h before N_2 adsorption. The specific surface areas were calculated from the Brunauer–Emmett–Teller (BET) equation.

X-ray photoelectron spectroscopy (XPS) was performed on an ULVAC PHI 5000 Versa Probe-II equipment operating at 10^{-9} Pa with an Al Ka radiation (1486.6 eV) to investigate and characterize the chemical states and surface atomic concentration of the samples. The observed spectra were referenced to the C 1 s binding energy value of 284.8 eV.

The NH_3 temperature-programmed desorption (NH_3-TPD) and the H_2 temperature-programmed reduction (H_2-TPR) experiments were employed on a GC-9750 with 0.03 g of the catalyst. Before the NH_3-TPD/H_2-TPR experiments, the catalysts were pretreated at 400 °C for 60 min in pure N_2 and cooled to the desired temperature. For the NH_3-TPD, the catalyst was cooled to 50 °C in pure N_2 followed by saturation for 40 min with a stream of NH_3(4%)/N_2. After saturation, the sample was flushed in a pure N_2 flow for 50 min at 100 °C. After that, the NH_3-TPD was operated in N_2 at a heating rate of 10 °C min^{-1} from 50 to 500 °C. As for H_2-TPR, The H_2-TPR runs were implemented in a flow of 5 vol% H_2/Ar (30 mL min^{-1}) from 100 to 700 °C with a heating rate of 10 °C min^{-1}. The NH_3 desorption (or H_2 uptake) was detected by a thermal conductivity detector (TCD).

Results and discussion

Catalytic performance of FeO_x, Fe–Mn–O_x and MnO_x catalysts

The catalytic activity and N_2 selectivity of FeO_x, Fe–Mn–O_x and MnO_x catalysts are shown in Fig. 1. It was found that the pure FeO_x had little activity in the temperature range of 50–150 °C. The MnO_x catalyst showed excellent SCR activity and over 85% of NO_x conversion at 125 °C. Fe–Mn–O_x exhibited a noticeable better catalytic activity than FeO_x and MnO_x, and above 80% NO_x conversion of Fe–Mn–O_x was acquired at 50–150 °C.

Figure 1b shows the N_2O concentration and N_2 selectivity of FeO_x, Fe–Mn–O_x and MnO_x catalysts. For FeO_x catalyst, it was hard to quantify the N_2 yield due to

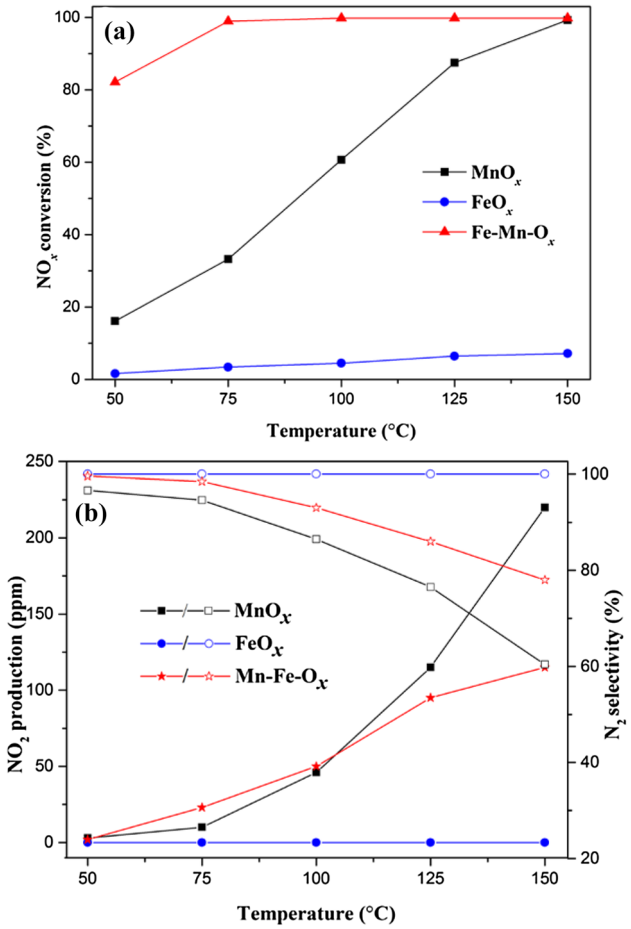

Fig. 1 Catalytic activity of the FeO_x, Fe–Mn–O_x and MnO_x catalysts. Reaction conditions: 600 ppm NO, 600 ppm NH_3, 5% O_2, balance N_2, GHSV = 60,000 h^{-1}. **a** NO_x conversion; and **b** N_2 selectivity

its poor catalytic activity. However, plenty of N_2O formed over the MnO_x catalyst. Furthermore, the amount of N_2O increased with the increase of the reaction temperature and the maximum of N_2O reached 220 ppm at 150 °C, which resulted in poor N_2 selectivity and the N_2 selectivity decreased sharply from 100 to 60%. As for Fe–Mn–O_x, the N_2 selectivity was significantly improved in comparison with that of MnO_x and nearly 80% N_2 selectivity was obtained at 150 °C. The phenomenon indicated that the introduction of Fe species into MnO_x could increase the low-temperature catalytic activity and N_2 selectivity.

XRD analysis

Figure 2 presents the XRD patterns of the FeO_x, Fe–Mn–O_x and MnO_x catalysts. As shown in Fig. 2, the diffraction peaks of tetragonal Mn_3O_4 phase (PDF: 80-0382) and cubic Mn_2O_3 phase (PDF: 78-0390) were observed in the XRD patterns of MnO_x catalyst. The diffraction peaks of hexagonal Fe_2O_3 phase (PDF: 89-0598) appeared for the FeO_x catalyst. As for Fe–Mn–O_x catalyst, the diffraction peaks of Mn_3O_4, Mn_2O_3 and Fe_2O_3 phase were not observed. The phenomenon indicated that Fe–Mn–O_x possessed low crystallization or Fe and Mn species existed as amorphous forms over Fe–Mn–O_x. Kharas et al. reported [26] that the low crystallization or amorphous forms of active species over NH_3-SCR catalysts could contribute to the improvement of catalytic activity. This might be a reason that Fe–Mn–O_x showed the best SCR performance among the samples.

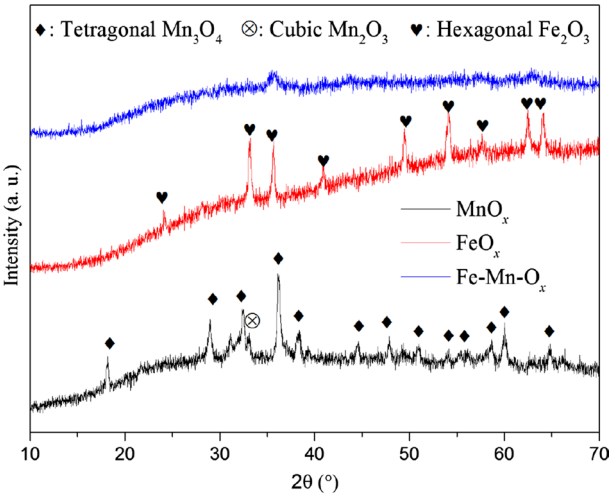

Fig. 2 Powder X-ray diffraction patterns of FeO_x, Fe–Mn–O_x and MnO_x catalysts

Raman analysis

To further study the structure of FeO_x, Fe–Mn–O_x and MnO_x catalysts, Raman spectra were operated and the results are shown in Fig. 3. The spectrum of FeO_x exhibited the Raman peaks at 1317, 611, 410, 295, 245 and 226 cm^{-1}, which could be assigned to Fe_2O_3 [8, 27, 28]. Furthermore, the peak at 503 cm^{-1} was observed, which was attributed to Fe_3O_4 [8, 27, 28]. For MnO_x, the MnO_2 (627, 540, 368 and 265 cm^{-1}), Mn_2O_3 (315 cm^{-1}) and Mn_3O_4 (657 and 485 cm^{-1}) were detected [8, 27, 28]. Besides, the intensity peak of Mn_3O_4 was much stronger than that of other Mn species, which was in good accord with XRD results. As for Fe–Mn–O_x catalyst, a broad weak peak centered at 650 cm^{-1} was observed, which proved the formation of Fe–O–Mn bands [8]. The phenomena implied that the addition of Fe species into MnO_x could affect the microstructure.

N_2 adsorption–desorption isotherms

Figure 4 shows the N_2 adsorption–desorption isotherms (a) and the BJH pore size distribution curves (b) of the FeO_x, Fe–Mn–O_x and MnO_x catalysts. According to IUPAC classification, it was obvious from the Fig. 4a that the samples presented type IV isotherms, which was assigned to the typically characteristic of mesopores (2–50 nm) [29]. Furthermore, the closure points of the hysteresis loops over MnO_x and FeO_x occurred when the value of P/P_0 was 0.87 and 0.81, respectively, while the value was 0.50 over Fe–Mn–O_x. The closure points of the hysteresis loops of Fe–Mn–O_x dramatically shifted to lower P/P_0 compared with that of MnO_x and FeO_x. The phenomenon suggested that more abundance of mesoporous was formed over Fe–Mn–O_x, which contributed to pore structure and BET specific areas, resulting in the improvement of catalytic activity in the NH_3-SCR reaction. Figure 4b

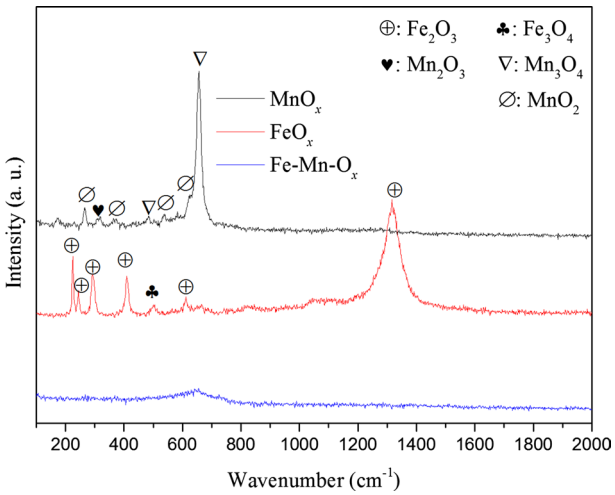

Fig. 3 Raman spectra of FeO_x, Fe–Mn–O_x and MnO_x catalysts

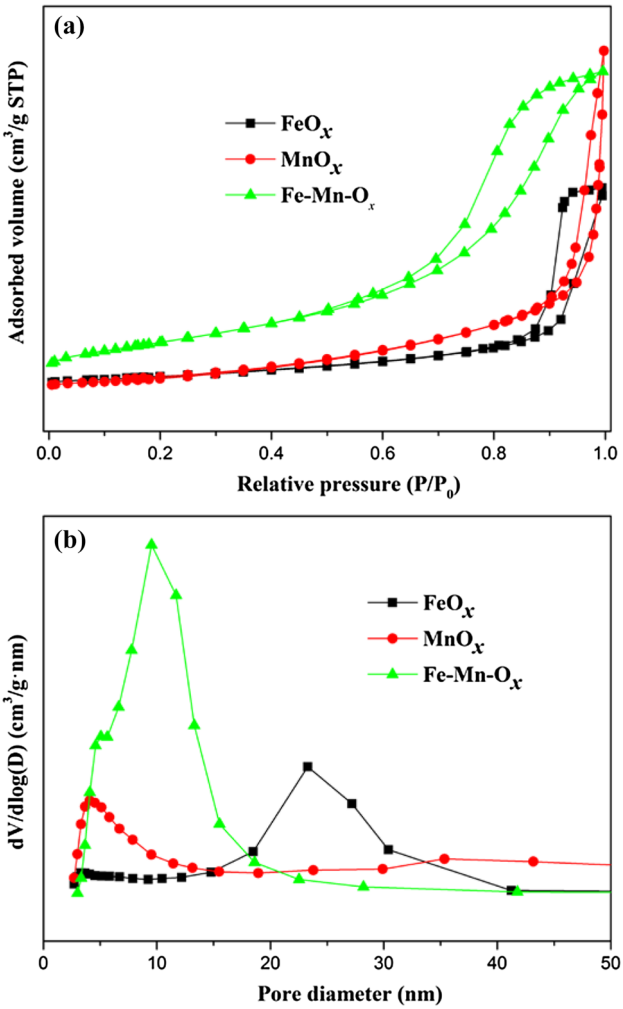

Fig. 4 N_2 adsorption–desorption results of the FeO_x, Fe–Mn–O_x and MnO_x catalysts: **a** the N_2 adsorption–desorption isotherms; **b** the BJH pore size distributions

shows the BJH pore size distributions of the FeO_x, Fe–Mn–O_x and MnO_x catalysts. It was clear that the main pore sizes of the three samples were distributed in the size range of 2–50 nm, which was assigned to the mesopore. The intensity of the peak over Fe–Mn–O_x was visibly higher than that of FeO_x and MnO_x, which implied that Fe–Mn–O_x possessed the most amount of mesopores among the samples, which could contribute to the favored pore structures and offered more active sites for the SCR reactions, leading to the enhancement of SCR performance.

Table 1 exhibits the BJH desorption pore volume and the BET surface area of the FeO_x, Fe–Mn–O_x and MnO_x catalysts. The total pore volume decreased: Fe–Mn–O_x (0.278 cm^3/g) > MnO_x (0.250 cm^3/g) > FeO_x (0.166 cm^3/g). Besides, the

Table 1 BET analysis results of FeO_x, Fe–Mn–O_x and MnO_x catalysts

Samples	BET (m^2/g)	Total pore volume (cm^3/g)
FeO_x	26	0.166
MnO_x	28	0.250
Fe–Mn–O_x	89	0.278

BET surface areas were 26, 28 and 89 m^2/g over the FeO_x, MnO_x and Fe–Mn–O_x, respectively. Combined with Fig. 4a, b results, it was inferred that the mesopores of FeO_x and MnO_x samples mainly presented in the inter-particle mesoporosity. In addition, the BET surface areas and total pore volume of Fe–Mn–O_x dramatically were increased compared with those of MnO_x and FeO_x, which demonstrated that the addition of Fe species into MnO_x over Fe–Mn–O_x could improve the pore structure of the Fe–Mn–O_x catalyst.

XPS analysis

The XPS spectra of Fe 2*p* for the FeO_x, Fe–Mn–O_x and MnO_x catalysts are shown in Fig. 5a. It was observed that the two peaks were located at about 709 and 723 eV, which could be attributed to Fe $2p_{3/2}$ and Fe $2p_{1/2}$, respectively [30]. Compared to FeO_x catalyst, the red shift in the binding energy was observed over Fe–Mn–O_x. The phenomenon proved that the interaction between Fe and Mn species existed, and then formed the Fe–O–Mn bond, which was demonstrated by Raman results. Besides, the satellite peaks centered at around 718 and 723 eV were observed, which implied that the Fe species consisted of Fe^{3+} and Fe^{2+} [31, 32]. In order to investigate the effect of Fe^{3+} and Fe^{2+} species on the catalytic activity and N_2 selectivity over Fe–Mn–O_x, the peaks of Fe 2*p* were fitted into six peaks for FeO_x and Fe–Mn–O_x. The peak positions of Fe 2*p* for Fe^{3+} species were located at about 711.5 and 725.3 eV, and the peaks at about 709.3 and 723 eV were attributed to the Fe^{2+} species [31, 32]. The relative amount of Fe^{3+} and Fe^{2+} was measured, and the results were shown in Table 2, the surface concentration of Fe^{3+} was about 30.9 and 37.5% over FeO_x and Fe–Mn–O_x catalyst, respectively. These suggested that the introduction of Fe species into MnO_x could improve the surface concentration of Fe^{3+}. Delahay et al. reported [33] that the oxidation step of NO to NO_2 was operated over Fe^{3+} sites in a NH_3-SCR reaction, which could accelerate the so-called "fast reaction", resulting in an improvement of catalytic activity, especially for the low-temperature SCR activity. Therefore, more amounts of Fe^{3+} could contribute to the formation of more NO_2. Fe–Mn–O_x catalyst with the highest Fe^{3+} (37.5%) surface concentration having the best catalytic performance at 50–150 °C, which was demonstrated by the results of NH_3-SCR activity.

The characteristic peaks for Mn 2*p* XPS spectra over MnO_x and Fe–Mn–O_x are presented in Fig. 5b. By performing a peak fitting deconvolution, the Mn $2p_{3/2}$ spectra appeared as three peaks: 640.6–641.8 (Mn^{2+} species), 642.3–643.6 (Mn^{3+} species) and 645–646 (Mn^{4+} species) eV, respectively [34]. Kapteijn et al. [35] reported

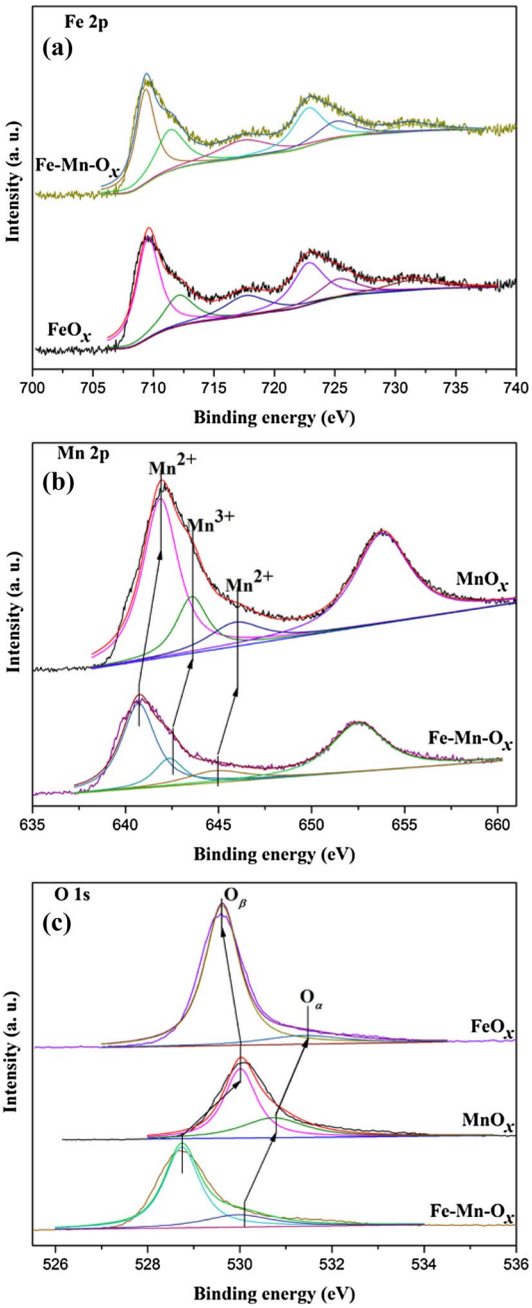

Fig. 5 **a** Fe 2*p* XPS spectra of FeO_x and Fe–Mn–O_x catalysts, **b** Mn 2*p* XPS spectra of MnO_x and Fe–Mn–O_x catalysts, **c** O 1*s* XPS spectra of the FeO_x, Fe–Mn–O_x and MnO_x catalysts

that Mn^{3+} species contributed to the improvement of N_2 selectivity, while Mn^{4+} could increase the catalytic activity, especially for the low-temperature SCR activity. However, the surface concentration of Mn^{3+} and Mn^{4+} over Fe–Mn–O_x decreased

Table 2 XPS results of FeO_x, Fe–Mn–O_x and MnO_x catalysts

Samples	Mn^{2+}	Mn^{3+}	Mn^{4+}	$Fe^{3+}/(Fe^{3+}+Fe^{2+})$	$O_\alpha/(O_\alpha+O_\beta)$
FeO_x	/	/	/	30.9	12.4
MnO_x	58.9	23.5	17.6	/	35.9
Fe–Mn–O_x	65.3	18.5	16.2	37.5	22.8

compared with that of MnO_x, and MnO_x possessed the inferior catalytic activity and poor N_2 selectivity at 50–150 °C. Lu et al. [36] proved that the co-existence of multiple valence Mn species was favored by the oxidation reduction reaction, resulting in the enhancement of low-temperature catalytic activity. Besides, the binding energy of Mn species of Fe–Mn–O_x shifted towards a lower value in comparison with that of MnO_x. This demonstrated that the strong interaction between Mn and Fe species existed, which could lead to an increasing in the outer electron cloud density of Mn species, and shielding effect improved. The phenomenon could improve the electron transfer ability, and then promoted the redox property. Therefore, the N_2 selectivity and catalytic performance of Fe–Mn–O_x and MnO_x should be further investigated.

Figure 5c presents the peak separation of the O 1*s* region for the FeO_x, Fe–Mn–O_x and MnO_x catalysts. The peak at 530.1–531.7 eV was assigned to chemisorbed oxygen O_α, and the lattice oxygen at 528.5–530.1 eV was denoted as O_β) [37, 38]. As shown in Fig. 4b, the ratio of $O_\alpha/(O_\alpha + O_\beta)$ over MnO_x and FeO_x was 35.9 and 12.4%, respectively. Fe–Mn–O_x possessed 22.8% $O_\alpha/(O_\alpha + O_\beta)$. It was reported [39] that higher chemisorbed oxygen (O_α) was favored by the outstanding SCR performance. However, the SCR performance of MnO_x was inferior compared with Fe–Mn–O_x. It was also well known that the over-oxidation ability of SCR catalysts could cause the ammonia oxidation, and then reduce the catalytic activity. This might be the reason that MnO_x with higher O_α concentration showed the poor SCR performance. Furthermore, the O_α and O_β binding energy for Fe–Mn–O_x was lower than that of the MnO_x and FeO_x, which suggested that the O_α and O_β of Fe–Mn–O_x possessed the most electron cloud density, leading to the generation of more reactive electrophilic oxygen species, which could remarkably enhance the catalytic activity of Fe–Mn–O_x [40].

H_2-TPR analysis

The H_2-TPR profiles of the FeO_x, Fe–Mn–O_x and MnO_x catalysts are exhibited in Fig. 6. It was found that FeO_x presented two reduction peaks at 394 and 622 °C, which was assigned to the reduction of Fe_2O_3–Fe_3O_4 (394 °C), Fe_3O_4–FeO (622 °C) [41–43], respectively. MnO_x exhibited two stages of reduction at 303 and 440 °C, which was interpreted as the reduction of Mn_2O_3–Mn_3O_4 and then to MnO, respectively [44]. The TPR curve of Fe–Mn–O_x showed the reduction peaks at 310, 460, and 560 °C. The reduction peak at 310 °C could correspond to the reduction of Mn_2O_3–Mn_3O_4. A broad peak centered at 460 °C could be attributed to the synergetic reduction of Fe_2O_3–Fe_3O_4 and Mn_3O_4–MnO. The phenomenon implied

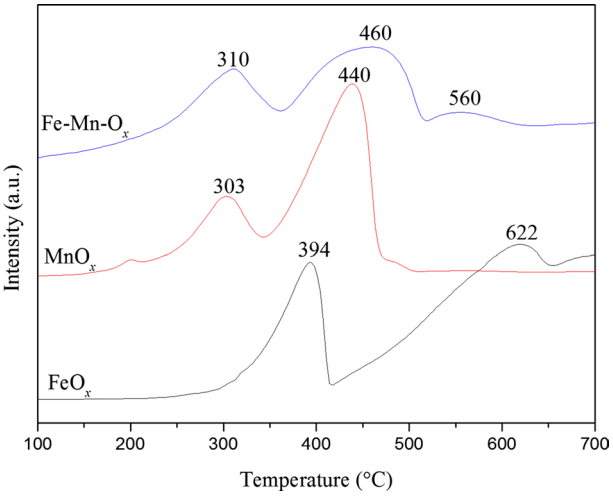

Fig. 6 H_2-TPR profiles of the FeO_x, Fe–Mn–O_x and MnO_x catalysts

that the interaction between Fe and Mn species over Fe–Mn–O_x existed. Besides, the reduction of Fe_3O_4–FeO over Fe–Mn–O_x shifted towards lower temperature in comparison with that of FeO_x. It was established that a shift in the peak position of the reduction temperature was closely related to many factors, such as a change in the amount of chemisorbed oxygen, structural defects and phase composition. The reduction temperature of Mn_2O_3–Mn_3O_4 over Fe–Mn–O_x moved to a higher value compared with that of MnO_x. Furthermore, the reduction temperature of Fe_3O_4–FeO over Fe–Mn–O_x was lower than that of FeO_x. These indicated that the redox property of Fe–Mn–O_x was induced in comparison with that of MnO_x but improved for FeO_x. Thereby, MnO_x showed the inferior catalytic activity due to the excellent redox ability, which could lead to the NH_3 oxidation to NO_x at high temperature. Combined with the Raman results, it was inferred that the presence of Mn–O–Fe species could increase the catalytic performance, which further confirmed that the interaction between Fe and Mn species occurred. Hence, the Fe–Mn–O_x catalyst exhibited the superior catalytic activity at 50–150 °C.

NH_3-TPD analysis

NH_3-TPD analysis was done in order to explore the influence of surface acidity on the catalytic performance and N_2 selectivity over FeO_x, Fe–Mn–O_x and MnO_x catalysts. As shown in Fig. 7, MnO_x showed one broad weak NH_3-desorption peak at 50–500 °C, which suggested that the MnO_x possessed the weak, medium and strong acid sites. For the FeO_x catalyst, it showed the NH_3-desorption peak at the temperature range of 100–500 °C, and the intensity of peak was higher than that of MnO_x, which indicated that the surface acidity of FeO_x catalyst was stronger than that of the MnO_x. It was observed that the NH_3-desorption peak of Fe–Mn–O_x was much stronger than those of FeO_x and MnO_x. The phenomenon implied that Fe–Mn–O_x

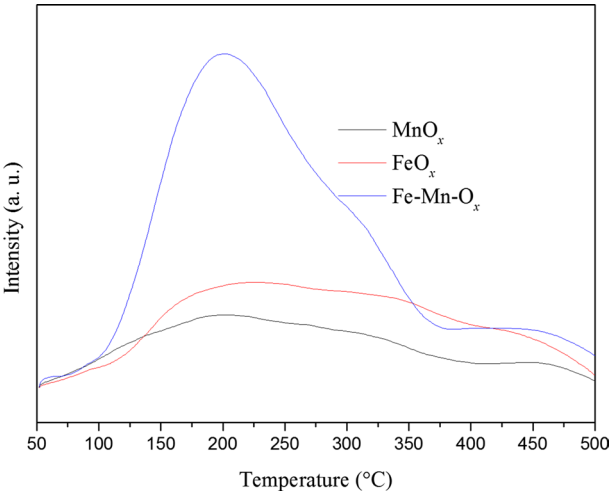

Fig. 7 NH_3-TPD profiles of the FeO_x, Fe–Mn–O_x and MnO_x catalysts

exhibited the most amount of surface acid sites, which might depend on the formation of Fe–O–Mn species. It was reported [8] that the presence of the $Fe_3Mn_3O_8$ phase (Fe–O–Mn species) could contribute to the improvement of surface acidity, and then improved the SCR performance. Consequently, the Fe–Mn–O_x catalyst showed the best catalytic activity at 50–150 °C among the samples. Besides, the peak of NH_3 desorption was spanned at 50–375 °C, proving that the Fe–Mn–O_x catalyst possessed more quantities of weak and medium acid sites. It was generally accepted that the improvement of the surface acidity of SCR catalysts could inhibit the oxidation of ammonia at high temperatures, and then promoted the catalytic activity and N_2 selectivity [45, 46]. Qu et al. reported [47] that the appropriate amounts of surface acid sites could adsorb and activate NH_3, which was thought to be the important steps for the reduction of NO with NH_3, and thus enhance the SCR performance and N_2 selectivity. Long et al. [48] also declared that the ammonia species could be adsorbed on acid sites to generate NH_4^+ ions and coordinated NH_3 species, and reacted with NO_x ad-species, leading to the superior catalytic performance. Therefore, the enhancement of surface acidity could improve the NH_3-adsorption capacity, and then increased the catalytic activity. Therefore, the surface acidity could improve the catalytic activity and N_2 selectivity over Fe–Mn–O_x catalyst.

Conclusions

Fe–Mn–O_x with high SCR activity and N_2 selectivity was prepared by the co-precipitation method. More than 80% NO_x conversion and nearly 80% N_2 selectivity were acquired in the temperature range of 50–150 °C. The surface species, the structure, the redox properties and the surface acidity were responsible for the excellent catalytic activity and N_2 selectivity. The formation of Fe–O–Mn species could improve

the SCR performance due to the enhancement of surface acidity, resulting in an increase in the catalytic activity and N_2 selectivity. Besides, the presence of Fe^{3+} and Mn^{4+} could contribute to the enhancement of low-temperature SCR activity, while Mn^{3+} was in favored for the superior N_2 selectivity over Fe–Mn–O_x catalyst. In addition, the interaction between Fe and Mn species existed and then accelerated the formation of surface acidity, leading to the improvement of low-temperature catalytic activity and N_2 selectivity.

Acknowledgements The project was supported by the National Program on Key Basic Research Project of China (973 Program, 2014CB643404), the National Natural Science Foundation of China (21567030 and 11447191) and the Natural Science Fund item of Yunnan Province under the Grant Number 2013FD033.

References

1. Y. Peng, W.Z. Si, X. Li, J.J. Chen, J.H. Li, J. Crittenden, J.M. Hao, Environ. Sci. Technol. **50**, 9576 (2016)
2. T. Boningari, P.G. Smirniotis, Curr. Opin. Chem. Eng. **13**, 133 (2016)
3. J.H. Li, H.Z. Chang, L. Ma, J.M. Hao, R.T. Yang, Catal. Today **175**(1), 147 (2011)
4. H.Z. Chang, L. Ma, S.J. Yang, J.H. Li, L. Chen, W. Wang, J.M. Hao, J. Hazard. Mater. **262**, 782 (2013)
5. Z. Song, P. Ning, Q. Zhang, X. Liu, J. Zhang, Y. Wang, Y. Duan, Z. Huang, J. Mol. Catal. A Chem. **413**, 15 (2016)
6. A. Grossale, I. Nova, E. Tronconi, D. Chatterjee, M. Weibel, J. Catal. **256**(2), 312 (2008)
7. C.J. Tang, H.L. Zhang, L. Hong, Catal. Sci. Technol. **6**(5), 1248 (2016)
8. Z. Chen, F. Wang, H. Li, Q. Yang, L. Wang, X. Li, Ind. Eng. Chem. Res. **51**, 202 (2012)
9. D.K. Pappas, T. Boningari, P. Boolchand, P.G. Smirniotis, J. Catal. **334**, 1 (2016)
10. P.R. Ettireddy, N. Ettireddy, T. Boningari, R. Pardemann, P.G. Smirnioti, J. Catal. **292**, 53 (2012)
11. B. Thirupathi, P.G. Smirniotis, Appl. Catal. B: Environ. **110**, 195 (2011)
12. P.G. Smirniotis, D.A. Peña, B.S. Uphade, Angew. Chem. Int. Ed. **40**, 2479 (2011)
13. M. Kang, E.D. Park, J.M. Kim, J.E. Yie, Appl. Catal. A **327**(2), 261 (2007)
14. Z. Chen, Q. Yang, H. Li, L. Wang, S.C. Tsang, J. Catal. **276**, 56 (2010)
15. B. Thirupathi, P.G. Smirniotis, J. Catal. **288**, 74 (2012)
16. M. Kang, E. Park, J. Kim, J.E. Yie, Catal. Today **111**, 236 (2006)
17. G. Qi, R.T. Yang, J. Catal. **217**, 434 (2003)
18. G. Qi, R.T. Yang, R. Chang, Appl. Catal. B **51**, 93 (2004)
19. S. Brandenberger, O. Kröcher, A. Wokaun, A. Tissler, R. Althoff, J. Catal. **268**, 297 (2009)
20. M. Schwidder, M.S. Kumar, U. Bentrup, J. Pérez-Ramírez, A. Brückner, W. Grünert, Micropor. Mesopor. Mater. **111**, 124 (2008)
21. S.H. Begum, C.T. Hung, Y.T. Chen, S.J. Huang, P.H. Wu, X.X. Han, S.B. Liu, J. Mol. Catal. A Chem. **423**, 423 (2016)
22. Z. Chen, X. Li, Y. Qing, H. Li, X. Gao, Y. Jiang, F. Wang, L. Wang, Acta Phys. Chim. Sin. **25**, 601 (2009)
23. L.J. France, Q. Yang, W. Li, Z.H. Chen, J.Y. Guang, D. Guo, L.F. Wang, X.H. Li, Appl. Catal. B Environ. **203–215**, 206 (2017)
24. R.Q. Long, R.T. Yang, R. Chang, Chem. Commun. **452**, 5 (2002)
25. Z.H. Chen, F.R. Wang, H. Li, Q. Yang, L.F. Wang, X.H. Li, Ind. Eng. Chem. Res. **202–212**, 51 (2012)
26. K.C.C. Kharas, Appl. Catal. B Environ. **2**, 207 (1993)
27. M.V. Reddy, T. Yu, C.H. Sow, Z.X. Shen, C.T. Lim, G.V. Subba Rao, B.V.R. Chowdari, Adv. Funct. Mater. **17**, 2792 (2007)
28. X.H. Nie, X.G. Li, C.W. Du, Y.Z. Huang, H. Du, J. Raman Spectrosc. **40**, 76 (2009)
29. B. Guan, H. Lin, L. Zhu, B. Tian, Z. Huang, Chem. Eng. J. **181–182**, 307 (2012)

30. T. Yamashita, P. Hayes, Appl. Surf. Sci. **254**, 2441 (2008)
31. S.J. Roosendaal, B. van Asselen, J.W. Elsenaar, A.M. Vredenberg, F.H.P.M. Habraken, Surf. Sci. **442**, 329 (1999)
32. S. Shwan, R. Nedyalkova, J. Jansson, J. Korsgren, L. Olsson, M. Skoglundh, Ind. Eng. Chem. Res. **51**, 12762 (2012)
33. G. Delahay, D. Valade, A. Guzman-Vargas, B. Coq, Appl. Catal. B Environ. **55**, 149 (2005)
34. G. Qi, R.T. Yang, J. Phys. Chem. B **108**, 15738 (2004)
35. F. Kapteijn, L. Singoredjo, A. Andreini, J.A. Moulijn, Appl. Catal. B **3**, 173 (1994)
36. X. Lu, C.Y. Song, C.C. Chang, Y.X. Teng, Z.S. Tong, X.L. Tang, Ind. Eng. Chem. Res. **53**, 11601 (2014)
37. Y.S. Eom, S.H. Jeon, T.A. Ngo, J. Kim, T.G. Lee, H. Catal. Lett. **121**, 219 (2008)
38. L. Chen, J.H. Li, M.F. Ge, Chem. Eng. J. **170**, 531 (2011)
39. Z.B. Wu, R.B. Jin, Y. Liu, H.Q. Wang, Catal. Commun. **9**, 2217 (2008)
40. F. Arena, G. Trunfio, J. Negro, B. Fazio, L. Spadaro, Chem. Mater. **19**, 2269 (2007)
41. G. Giecko, T. Borowiecki, W. Gac, J. Kruk, Catal. Today **137**, 403 (2008)
42. M.R. Morales, B.P. Barbero, L.E. Cadús, Appl. Catal. B **74**, 1 (2007)
43. K. Sirichaiprasert, A. Luengnaruemitchai, S. Pongstabodee, Int. J. Hydrogen Energy **32**, 915 (2007)
44. S.P. Dey, S. Gedevanishvili, W. Zhang, F. Rasouli, Appl. Catal. B **56**, 241 (2005)
45. Z.C. Si, D. Weng, X.D. Wu, R. Ran, Z.R. Ma, Catal. Commun. **11**, 1045 (2010)
46. L. Chen, J.H. Li, M.F. Ge, R.H. Rong, Catal. Today **153**, 77 (2010)
47. R.Y. Qu, X. Gao, K.F. Cen, J.H. Li, Appl. Catal. B Environ. **142–143**, 290 (2013)
48. R.Q. Long, R.T. Yang, J. Catal. **190**, 22 (2000)